



## OPEN **Neurons of the precuneiform nucleus share structural and functional properties of the mesencephalic locomotor region**

K. Pocsai<sup>1,4</sup>, T. Bayasgalan<sup>1,3,4</sup>, A. Csemer<sup>1</sup>, P. Szücs<sup>2</sup>, J. Mena-Segovia<sup>3</sup> & B. Pál<sup>1</sup>✉

The mesencephalic locomotor region (MLR) encodes a diverse range of movements, from locomotion to posture and turning behavior. While the cuneiform nucleus (CnF) and pedunculopontine nucleus (PPN), the main components of the MLR, have been recently characterized, little is known about the precuneiform nucleus (PrCnF). To address this gap, we performed somatodendritic morphological analyses and *ex vivo* functional studies on PrCnF neurons of VGluT2-tdTomato mice and compared them with those of neighboring MLR nuclei. PrCnF neurons exhibited dendritic morphology similar to PPN neurons but distinct from CnF neurons. Functionally, PrCnF neurons displayed higher firing rates and oscillatory activity compared to CnF and PPN neurons, which were correlated with TTX-sensitive high-threshold membrane potential oscillations mediated by the persistent Na<sup>+</sup> current present in most PrCnF neurons. Unlike PPN and CnF neurons, the majority of PrCnF neurons did not show depolarization-related changes in spike frequency adaptation, indicating that their intrinsic properties support continuous high-frequency spiking. These findings suggest that PrCnF neurons may have a uniform relationship to movement speed similar to CnF neurons and that activation of the PrCnF might be related to higher-speed movements due to their weak spike frequency adaptation and higher firing rates.

**Keywords** Precuneiform nucleus, Pedunculopontine nucleus, Cuneiform nucleus, Glutamatergic neuron, Somatodendritic parameters, Membrane properties

The mesencephalic locomotor region (MLR) of the midbrain is an evolutionarily conserved area of the brain from rodents to primates. The region consists of the pedunculopontine (PPN), cuneiform nuclei (CnF), the precuneiform nucleus (PrCnF) and the mesencephalic reticular formation<sup>1,2</sup>. Electric or optogenetic stimulation of the PPN and CnF increase the muscle tone and initiate or stop locomotion<sup>3–6</sup>. The nuclei that compose the MLR do not only contribute to movement regulation but also to cardiovascular and respiratory functions<sup>7,8</sup>, modulate the transitions to wakefulness and REM sleep<sup>6</sup>, and contribute to the recovery of incomplete spinal cord injuries in mice<sup>9</sup>.

Among the neurons that compose the MLR, the glutamatergic neurons of the PPN and CnF have been characterized in terms of their *in vitro* and *in vivo* physiological properties and their morphological and connectivity features<sup>5,9–14</sup>. However, the neurons composing the PrCnF are poorly described. Situated rostral to the CnF and dorsal to the PPN, it has been shown to have similarities in the morphology, projection and functions among other MLR structures, as described in the monkey and the cat<sup>1,8,15</sup>. PrCnF neurons receive inputs from the central amygdala, likely encoding cardiovascular and vasomotor signals<sup>8</sup>, and in turn target central pattern generators in the ipsilateral cervical and thoracic spinal cord<sup>1,15</sup>, thus highlighting its potential significance as an output structure of the MLR relaying central autonomic signals to other motor circuits.

In this study we demonstrate that the majority of PrCnF glutamatergic neurons display a variety of electrophysiological properties similar to PPN and CnF glutamatergic neurons, whereas a subset of PrCnF neurons display unique electrophysiological properties compared to the rest neurons in the MLR. The biophysical similarities among MLR neurons suggest shared dynamical properties associated with their spatial position within the MLR.

<sup>1</sup>Department of Physiology, Faculty of Medicine, University of Debrecen, Debrecen, Hungary. <sup>2</sup>Department of Anatomy, Histology and Embryology, Faculty of Medicine, University of Debrecen, Debrecen, Hungary. <sup>3</sup>Center for Molecular and Behavioral Neuroscience, Rutgers University, Newark, NJ 07102, USA. <sup>4</sup>K. Pocsai and T. Bayasgalan contributed equally to this work. ✉email: pal.balazs@med.unideb.hu

## Results

### Somatodendritic properties

Neurons of the PrCnF were distinguished from the PPN and the CnF on the basis of the dorsoventral and rostrocaudal location of the soma (Fig. 1A). Only tdTomato-expressing somata (i.e., glutamatergic) located within 3 mm dorsally to the brain surface and  $-4.72$  mm rostral to bregma were considered as glutamatergic neurons of the PrCnF<sup>16</sup>. Neurons situated caudally to the PrCnF were considered CnF neurons whereas ventral neurons were considered PPN neurons. Based on this spatial segregation, we reconstructed individual neurons of the PrCnF ( $n = 9$ ), CnF ( $n = 9$ ) and PPN ( $n = 13$ ) (Fig. 1B–D). Data from neurons of the PPN and CnF were previously published<sup>5</sup>. In this work, we re-analyzed and compared them with the novel data from the PrCnF.

We obtained the following somatodendritic parameters: number of dendrites, dendritic nodes (branching points), ends and spines, and soma area, and we compared them between the three MLR structures. The number of dendrites were similarly low in the PrCnF and the PPN (Figs. 1E and  $3.11 \pm 0.22$  and  $3.66 \pm 0.33$ , respectively), whereas CnF neurons had a significantly higher number of dendrites ( $5.11 \pm 0.43$ ; CnF vs. PrCnF:  $p = 0.0013$ ; CnF vs. PPN:  $p = 0.0125$ ; PrCnF vs. PPN: n.s.). The total dendritic length was  $693.76 \pm 122.26$   $\mu\text{m}$  for the PrCnF,  $1407.47 \pm 234.06$   $\mu\text{m}$  for the CnF and  $1106.08 \pm 177.43$   $\mu\text{m}$  for the PPN ( $p = 0.03$  for PrCnF vs. CnF, Fig. 1E). The dendritic nodes had a low number in the PrCnF ( $4.66 \pm 0.87$ ) but higher in the CnF and PPN (CnF:  $15 \pm 4.38$ ; PPN:  $8.08 \pm 1.51$ ; CnF vs. PrCnF:  $p = 0.028$ , PrCnF vs. PPN: n.s.; CnF vs. PPN: n.s.; Fig. 1E). A similar (and expected) tendency was seen with the dendritic ends (Fig. 1E; PrCnF:  $8 \pm 0.93$ , PPN:  $11.58 \pm 1.73$ , CnF:  $20 \pm 4.56$ ; PrCnF vs. PPN: n.s., PrCnF vs. CnF:  $p = 0.0153$ ; CnF vs. PPN: n.s.). We did not find a significant difference or any tendency in the soma area ( $181.12 \pm 25.83$   $\mu\text{m}^2$  in the PrCnF,  $228.71 \pm 50.16$   $\mu\text{m}^2$  in the CnF and  $182.78 \pm 15.87$   $\mu\text{m}^2$  in the PPN; Fig. 1E). PrCnF neurons showed a low number of dendritic spines ( $7.33 \pm 1.97$ ); in contrast, in the CnF, the numbers were more heterogeneous: some neurons showed a large number of spines (61–132), whereas other neurons have only a few. This dichotomy accounts for the greater standard error ( $32.11 \pm 15.09$  in average) and the lack of significant difference. The number of dendritic spines is also numerically higher in the PPN than the PrCnF ( $28.83 \pm 8.7$ ; Fig. 1E). However, no significant difference in spine density was seen between the PrCnF and other nuclei ( $0.0091 \pm 0.026/\mu\text{m}$  in the PrCnF,  $0.022 \pm 0.0094/\mu\text{m}$  in the CnF and  $0.027 \pm 0.008/\mu\text{m}$  in the PPN; Fig. 1E).

Sholl analysis revealed significant differences between the PrCnF and other MLR nuclei. We found differences in the length ( $p = 0.044$  between PrCnF and PPN at  $130$   $\mu\text{m}$ ), in the intersections ( $p = 0.031$  at  $70$   $\mu\text{m}$ ;  $p = 0.023$  at  $80$   $\mu\text{m}$ ;  $p = 0.0304$  between PrCnF and PPN and PrCnF and CnF at  $110$   $\mu\text{m}$ ; Fig. 1F), and in the spines ( $p = 0.0499$  at  $190$   $\mu\text{m}$  between PrCnF and PPN). No significant differences in nodes and endings were observed. In summary, the somatodendritic morphology of PrCnF neurons is similar to PPN neurons than to CnF neurons. The dendritic arborization of PrCnF neurons is lower than in CnF neurons but similar to PPN neurons. PrCnF neurons have a few dendritic spines whereas neuronal subpopulations of the PPN and CnF neurons possess abundant spines.

### Electrophysiological properties

Neurons in the MLR differ in their morphological, neurochemical and biophysical properties<sup>5,6,17</sup>. The 'classical' biophysical characterization is based on the absence or presence of low threshold calcium spikes (LTS) or rebound spikes, as well as the delay of the first action potential (AP) in the train (at  $-80$  mV resting membrane potential). If only LTS is present, the cell is considered as type (I) Cells with first AP delay but not LTS belong to type (II) If both properties are present, the neuron is classified as type III; if none, type IIIK<sup>5,10,14</sup> (Fig. 2A–C). In the PrCnF, 17.4% of the glutamatergic neurons were type I. Type II and III were equally present with 30.45%, whereas 21.7% belonged to type IIIK. This means that LTS is present in approximately half of the PrCnF population (47.8%), whereas the first AP delay is seen on almost two-third of the PrCnF cells (60.9%;  $n = 23$ ; Fig. 2D–F). In comparison, in the PPN, 22.7% of the glutamatergic neurons were type I, 43.2% were type II, 9.1% were type III and 25% were type IIIK. 31.8% of the neurons had LTS and 52.3% displayed AP delay ( $n = 44$ ;<sup>5</sup>. In the CnF, 33.3% of neurons were type I, 37.5% were type II, 16.7% were type III and 12.5% were type IIIK. 50% of the cells had LTS and 54.2% had AP delay ( $n = 24$ ; Fig. 2D–F).

Cholinergic neurons of the PPN have a delay of the first AP from  $-80$  mV resting membrane potential, directly correlating with the decay tau of the A-current<sup>14</sup>. We found this correlation to be also present in PrCnF neurons. Namely, if the decay tau of the A-current increased, the delay of the first action potential was increased too ( $r^2 = 0.641$ ,  $p = 0.0006$ ). Notably, this correlation was absent in PPN and CnF glutamatergic neurons (PPN:  $r^2 = 0.0222$ ,  $p = 0.595$ ; CnF:  $r^2 = 0.101$ ,  $p = 0.248$ ). In summary, there is a slightly higher proportion of neurons with AP delay and the presence of A-current in the PrCnF, but otherwise there is no fundamental difference between the proportions of 'classical' functional cell types across the MLR.

Next, we defined functional cell types based on spike adaptation. 'Non-adapting' neurons have less than 50% increase in the adaptation index of the action potential trains obtained with 50 and 120 pA current injections (Fig. 2G); 'slowly adapting' neurons have more than 50% change of the adaptation index (Fig. 2H), but fired during the whole 1-s-long depolarizing step, whereas 'fast adapting' neurons pause firing after application of greater depolarizing steps (Fig. 2I;<sup>5</sup>. In the PrCnF, the dominant functional cell type was the non-adapting type (65.22%), whereas 26.09% of neurons were fast adapting and 8.7% were slow adapting. In contrast, the dominant functional type of the CnF was fast adapting (85.71%) and an equal number of non-adapting and slow adapting (7.14 and 7.14%, respectively). The PPN displayed the largest heterogeneity with 50% of fast adapting, 18.42% of slow adapting and 31.58% of non-adapting glutamatergic neurons<sup>5</sup>; Fig. 2J). However, no significant difference was revealed between nuclei in the adaptation index recorded at 100 pA depolarizing step (PrCnF:  $0.406 \pm 0.035$ ,  $n = 22$ ; CnF:  $0.383 \pm 0.048$ ,  $n = 11$ ; PPN:  $0.319 \pm 0.036$ ,  $n = 29$ ).

The average action potential firing rate elicited by 100 pA depolarizing step was also investigated. We found that the firing rate of PrCnF neurons was significantly higher than in the PPN and CnF (PrCnF:  $17.33 \pm 1.59$  Hz,

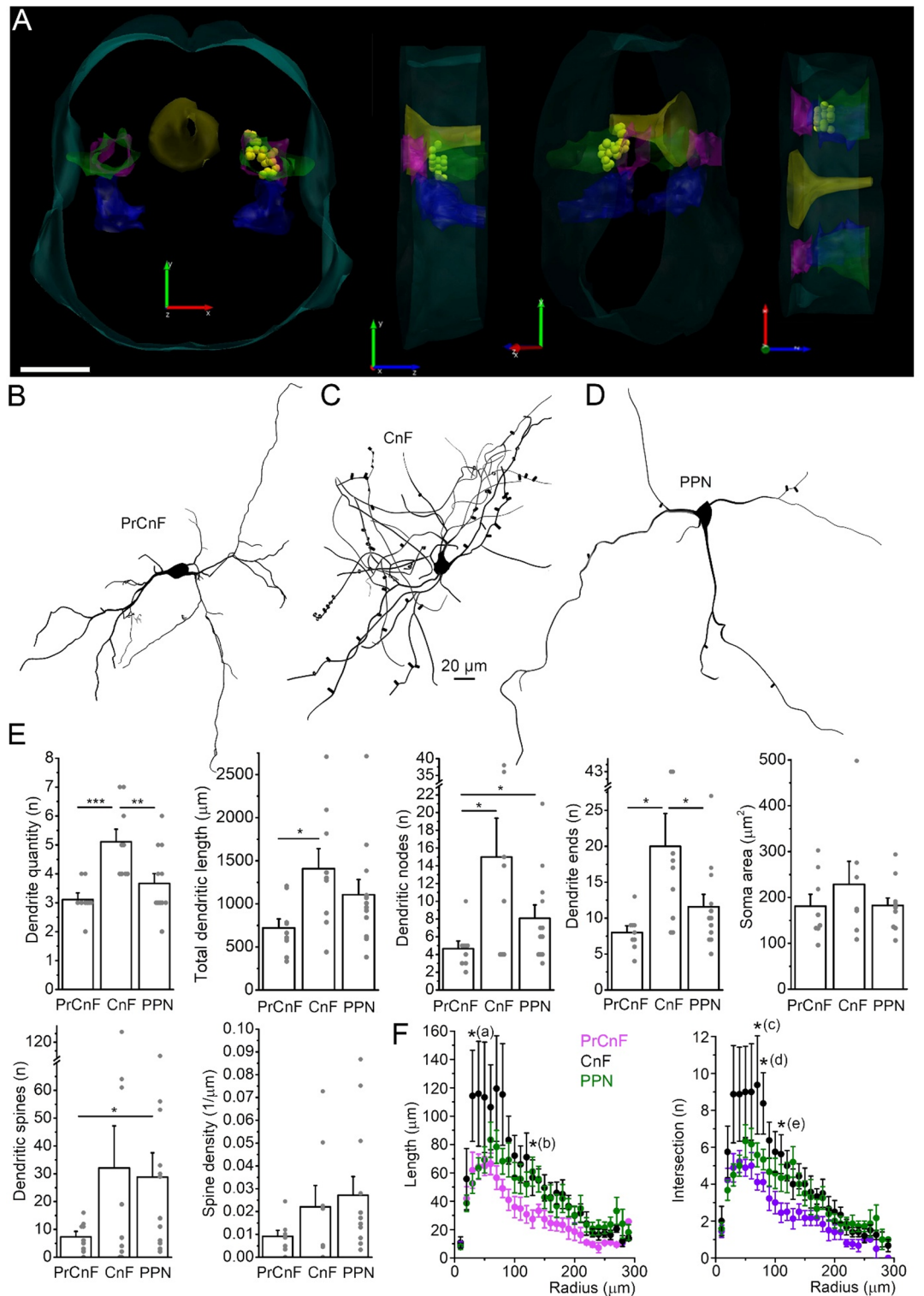


**Fig. 1.** Comparison of the somatodendritic morphology of mesencephalic locomotor region (MLR) nuclei. **A.** Location of the recorded PrCnF somata (yellow spheres: location of somata; green contour: PrCnF, purple contour: CnF, blue contour: PPN, yellow contour: aqueduct; green arrow: dorsal direction, red arrow: left, blue arrow: rostral). Scale bar: 1 mm. **B–D.** Representative images of reconstructed glutamatergic neurons of the precuneiform nucleus (PrCnF; **B**), the cuneiform nucleus (CnF; **C**) and the pedunculo pontine nucleus (PPN; **D**). Scale bar for A–C: 20  $\mu\text{m}$ . **E.** Statistical comparison of various somatodendritic parameters of the three nuclei listed above (columns: average  $\pm$  SEM; gray dots: individual data; \*,  $p < 0.05$ ; \*\*,  $p < 0.01$ ; \*\*\*,  $p < 0.001$ ). **F.** Statistical comparison of the Sholl analysis of the dendritic length and intersections of the PrCnF (purple), the CnF (black) and the PPN (red; average  $\pm$  SEM, \*,  $p < 0.05$ ; a:  $p = 0.02$ , CnF vs. PPN; b:  $p = 0.044$ , PrCnF vs. PPN; c:  $p = 0.031$  both for PrCnF vs. CnF and PrCnF vs. PPN; d:  $p = 0.023$  both for PrCnF vs. CnF and PrCnF vs. PPN; e:  $p = 0.0304$  both for PrCnF vs. CnF and PrCnF vs. PPN).

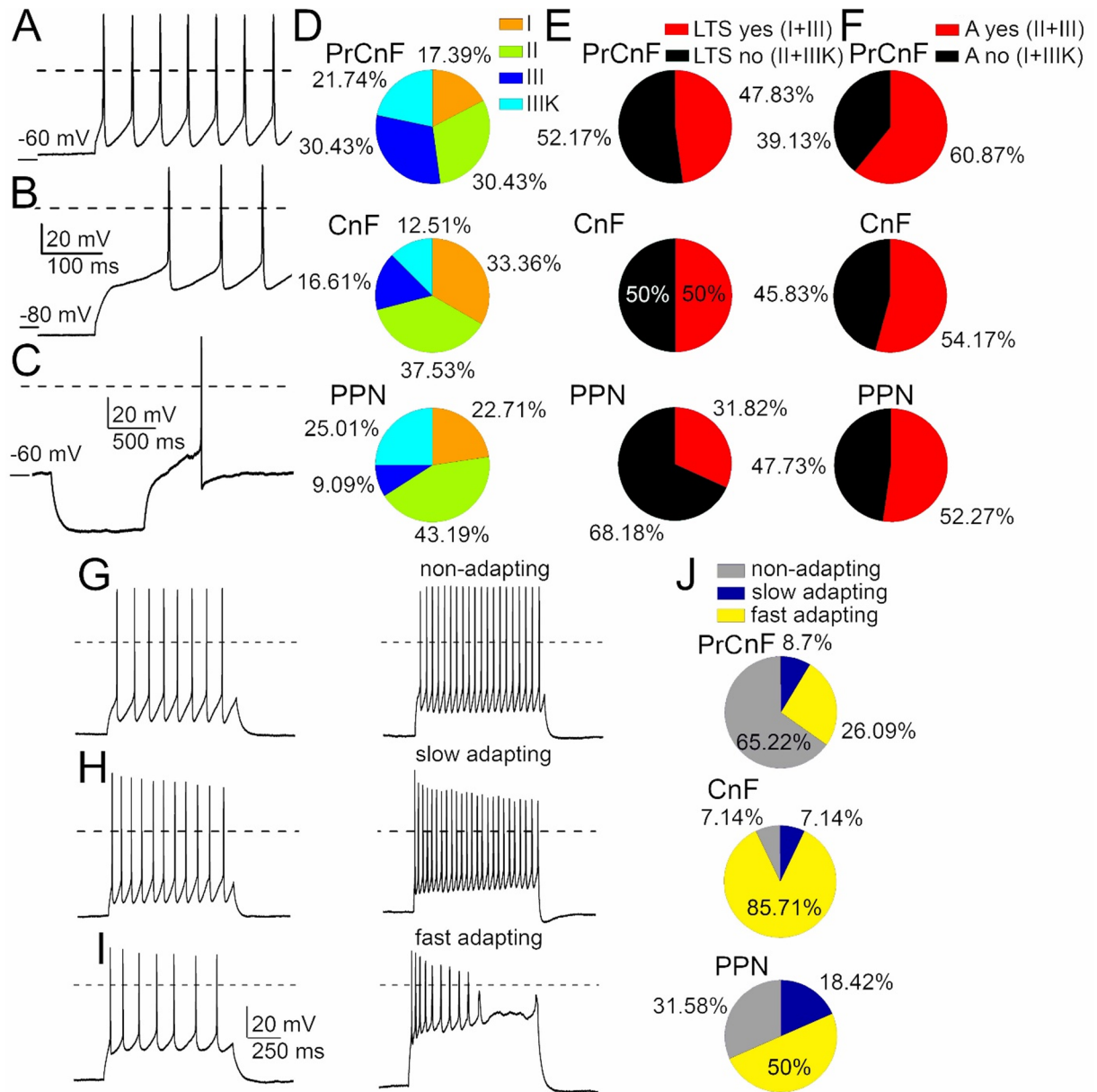


**Fig. 2.** Functional cell properties across MLR nuclei. **A–F.** Proportions of classical electrophysiological cell types sorted on the basis of the presence of the first AP delay/A-current and low threshold calcium spikes/rebound spikes. **A–B.** Action potential trains elicited with 100 pA depolarizing square pulse from  $-60$  and  $-80$  mV resting membrane potentials. Note the delay of the first AP on panel B. **C.** A rebound spike elicited at the end of  $-30$  pA hyperpolarizing pulse from  $-60$  mV. **D.** Proportions of functional cell types in the precuneiform nucleus (PrCnF), cuneiform nucleus (CnF) and the pedunclopontine nucleus (PPN). Type I: Only low threshold spike (LTS); II: only AP delay/A-current; III: both; IIK: none of them. **E.** Proportions of neurons with or without low threshold spikes (LTS) or rebound spikes (C). **F.** Proportions of neurons with or without first AP delay/A-current (A–B). **G–J.** Proportions of neurons based on changes in spike frequency adaptation. **G–I.** Representative voltage traces elicited with 50- and 100 pA depolarizing square current protocols on non-adapting (G), slow adapting (H) and fast adapting (I) neurons. The dashed lines indicate 0 mV. **J.** Proportions of non-adapting, slow- and fast adapting neurons.

$n=24$ ; CnF:  $11.74 \pm 1.89$  Hz,  $n=23$ ; PPN:  $12.42 \pm 1.18$ ;  $n=31$ ; CnF vs. PrCnF:  $p=0.0347$ ; PPN vs. PrCnF:  $p=0.0495$ ; PPN vs. CnF: n.s.). Taken together, based on the depolarization-induced changes of the adaptation index and firing rate, the PrCnF has key functional differences compared to the other nuclei of the MLR (Fig. 3A–B).

Next, we investigated the currents determining neuronal excitability that are not included in the definition of the functional groups described above. First, we compared the proportion of neurons having M-current across MLR neurons. Neurons having greater than 20 pA relaxation current at  $-40$  mV repolarizing voltage step are

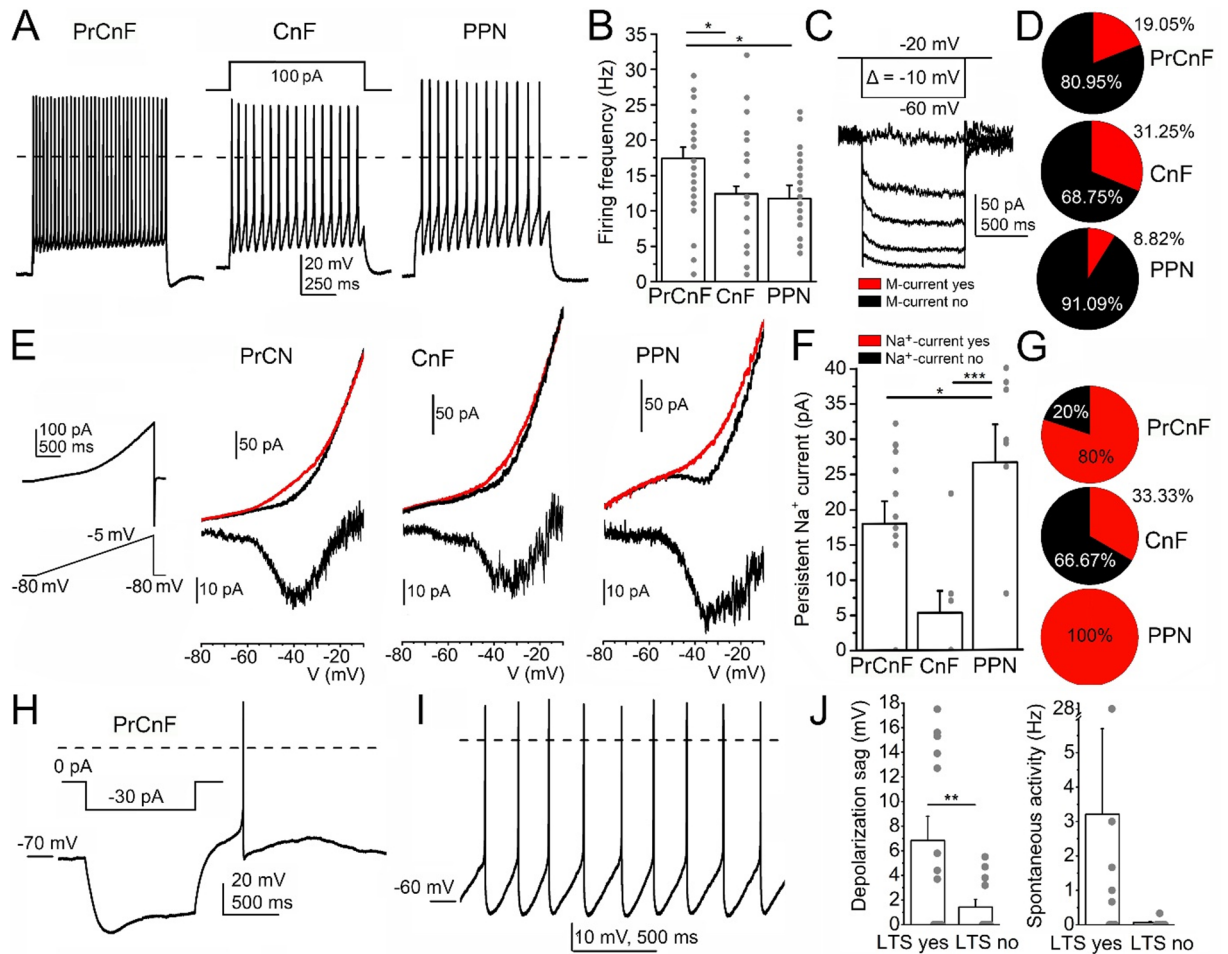
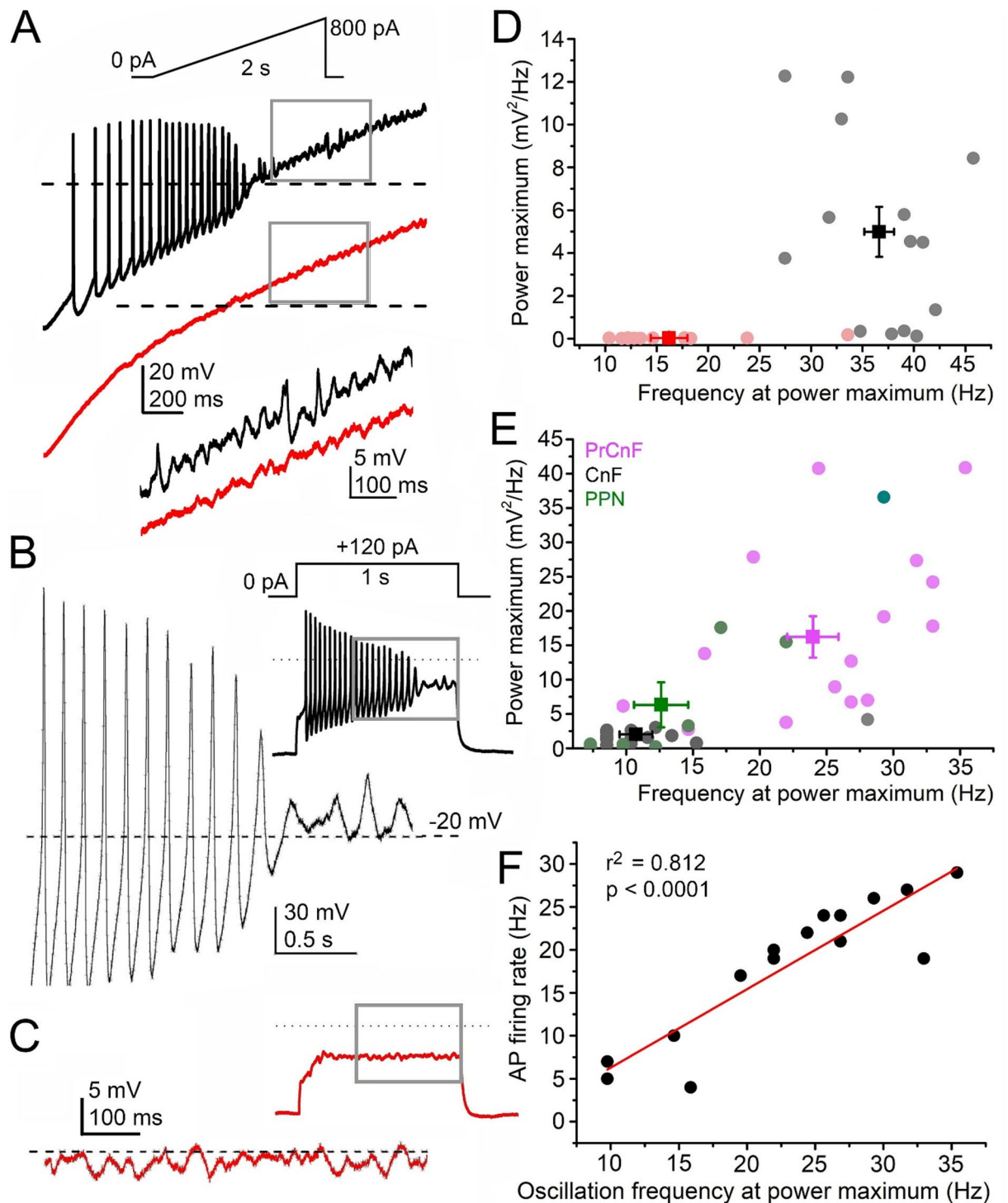


**Fig. 3.** Differences in membrane properties of MLR neurons. **(A)** Representative action potential trains elicited by 100 pA depolarizing square current pulses from glutamatergic neurons of the PrCnF, CnF and PPN, respectively. The dashed lines indicate 0 mV. **(B)** Statistical comparison of the firing frequency in different nuclei (columns: average  $\pm$  SEM; gray dots: individual data;  $^*p < 0.05$ ). **(C)** Representative current traces of the M-current recorded with M-current relaxation protocol ( $-20$  mV holding potential with repolarizing steps from  $-60$  mV with  $10$  mV increment). **(D)** Pie charts showing the proportions of glutamatergic neurons with or without M-current (red and black, respectively). **(E)** Persistent sodium currents of the different nuclei. Black traces: control, red traces: after TTX treatment, inserts below: TTX-sensitive currents. **(F)** Statistical comparison of the amplitude of the persistent sodium current (columns: average  $\pm$  SEM; gray dots: individual data;  $^*p < 0.05$ ;  $^{***}p < 0.001$ ). **(G)** Pie charts demonstrating the proportions of glutamatergic neurons with or without persistent sodium current (red and black, respectively). **(H)** A depolarization sag and a rebound spike of a PrCnF neuron elicited with  $30$  pA hyperpolarizing square current injection. **(I)** Spontaneous action potential firing of a PrCnF neuron. **(J)** Statistical comparison of the depolarization sag amplitude and the spontaneous action potential firing rate of neurons possessing or lacking low threshold spikes (columns: average  $\pm$  SEM; gray dots: individual data;  $^*p < 0.01$ ).

considered as possessing M-current. We found that in the PrCnF, 19.05% of the neurons had M-current (4 from 21), 31.25% in the CnF (10 from 33) and 8.82% in the PPN (3 from 34; 2 of which also expressed ChAT). The average relaxation current amplitude (including the cases with no M-current) at  $-40$  mV repolarizing voltage step was  $7.89 \pm 2.79$  pA in the PrCnF,  $11.51 \pm 2.42$  pA in the CnF and  $6.04 \pm 1.71$  pA in the PPN (n.s.; Fig. 3C-D).

We have previously showed the presence of persistent sodium current in the PPN and CnF. Here we found that 80% of the PrCnF neurons displayed persistent sodium current, compared to 100% in the PPN and 33.33% in the CnF (Fig. 3E-G). In PrCnF neurons, the current amplitude was  $18 \pm 3.21$  pA ( $n = 13$ ) whereas in CnF neurons it was  $5.31 \pm 3.12$  pA and in the PPN  $26.6 \pm 5.41$  pA ( $n = 7$  and  $9$ , respectively; PrCnF vs. PPN,  $p = 0.0208$ ; PrCnF-CnF, n.s.; CnF - PPN,  $p = 0.0002$ ; Fig. 3E-G).

In 46.15% of all cases (12 from 26), PrCnF neurons displayed depolarization sag with an amplitude of  $7.94 \pm 1.76$  mV (ranging from 3.2 to 17.5 mV; Fig. 3H). In contrast, the depolarization sag occurred with a lower probability in the CnF and PPN. In the CnF, only 6.06% (2 from 34) possessed it with a similar average amplitude as in the PrCnF ( $8.3 \pm 3.1$  mV, ranging from 5.2 to 11.4 mV). In the PPN, this phenomenon was also less frequent, as 19.56% (9 from 46) possessed it (average amplitude:  $7.22 \pm 1.02$  mV, from 4.1 to 13.7 mV).



In 36.36% of the cases (8 from 26), PrCnF neurons also displayed spontaneous activity with a frequency of  $4.5 \pm 3.37$  Hz (ranging from 0.33 to 28 Hz; Fig. 3I). In the CnF, only 9.37% (3 from 33) of the neurons had spontaneous activity with a frequency of  $0.88 \pm 0.4$  Hz (from 0.33 to 1.66 Hz). In the PPN, 6.67% had spontaneous activity with a frequency of  $0.66 \pm 0.19$  Hz (0.33–1 Hz).

On PrCnF neurons, the presence or absence of the LTS was related to the depolarization sag but not to the spontaneous activity. Neurons possessing LTS had an average depolarization sag of  $6.84 \pm 1.96$  mV, whereas in the ones lacking LTS had significantly lower amplitude ( $1.43 \pm 0.63$  mV including the cases without depolarization sag;  $p = 0.009$ ; Fig. 3J). However, the spontaneous activity did not significantly differ between neurons possessing or lacking LTS ( $3.21 \pm 2.49$  Hz on neurons with and  $0.06 \pm 0.04$  Hz without LTS; Fig. 3J).

We previously demonstrated that the vast majority of the cholinergic neurons had TTX-resistant high threshold membrane potential oscillations<sup>14,18</sup> but the glutamatergic ones almost lacked it (with the exception of cholinergic markers<sup>5</sup>). In the PrCnF, we found the presence of TTX-sensitive high threshold membrane potential

◀ **Fig. 4.** Membrane potential oscillations in the precuneiform nucleus. **(A)** TTX-resistant membrane potential oscillations in PrCnF neurons. Representative voltage traces elicited with depolarizing ramp protocol (see above the voltage trace) under control conditions (black) and with TTX (red). The inserts represent magnifications of areas indicated with the gray squares. Dashed lines represent 0 mV. **B-C.** TTX-sensitive and -resistant oscillations in the PrCnF elicited by depolarizing square pulses (see above the voltage trace of panel B). **(B)** Representative voltage trace under control conditions elicited with 100 pA square current pulses. The gray square on the insert indicates the magnified area of the main trace on the panel. The dashed line indicates -20 mV. **(C)** Voltage traces recorded under the same conditions as on panel C except that TTX was applied. **(D)** Comparison of oscillatory frequencies and power maxima under control conditions (gray dots: individual data, black square: average  $\pm$  SEM) and with TTX (pink dots: individual data, red square: average  $\pm$  SEM). **(E)** Comparison of frequencies and power amplitudes of TTX-sensitive oscillatory activities in the PrCnF, CnF and PPN. (PrCnF: magenta dots: individual data, magenta square: average  $\pm$  SEM; CnF: gray dots: individual data, black square: average  $\pm$  SEM; PPN: blue dots: individual data, blue square: average  $\pm$  SEM) **(F)** Correlation between the frequency of the TTX-sensitive oscillations and action potential firing rate in the PrCnF. Black dots: individual data, red line: linear fit.

oscillations. By analyzing the membrane potential changes above 0 mV that were elicited by depolarizing current injections, we found that PrCnF glutamatergic neurons possess oscillatory activity with a frequency of  $36.62 \pm 1.45$  Hz and  $4.99 \pm 1.17$  mV<sup>2</sup>/Hz power. When TTX was applied, the oscillations almost disappeared (power:  $0.035 \pm 0.012$  mV<sup>2</sup>/Hz; frequency:  $16.2 \pm 1.78$  Hz;  $n = 14$ ; PrCnF vs. PPN,  $p = 0.0191$ ; PrCnF-CnF,  $p < 0.0001$ ; CnF - PPN, n.s.; Fig. 4A-B). Compared to the other MLR nuclei, the PrCnF had the highest frequency and power of TTX-sensitive membrane potential oscillations elicited by square current injections ( $23.98 \pm 1.92$  Hz frequency,  $16.23 \pm 3.01$  mV<sup>2</sup>/Hz power;  $n = 17$ ). In the PPN, the oscillatory frequency was  $12.61 \pm 2.03$  Hz, whereas the power was  $6.33 \pm 3.28$  mV<sup>2</sup>/Hz ( $n = 12$ ), and in the CnF, it was  $10.72 \pm 1.22$  Hz, the power was  $2.03 \pm 0.99$  mV<sup>2</sup>/Hz ( $n = 19$ ; PrCnF vs. PPN,  $p < 0.0001$ ; PrCnF-CnF,  $p < 0.0001$ ; CnF - PPN, n.s.; Fig. 4C-E). The frequency of the TTX-sensitive membrane potential oscillations showed a correlation with the action potential firing rate: when the oscillatory frequency increased, the action potential firing rate was also increased (slope = 0.91;  $r^2 = 0.811$ ;  $p < 0.0001$ ;  $n = 15$ ; Fig. 4F).

### Integration of functional and morphological properties of PrCnF neurons

Next, we made a series of comparisons using the parameters obtained from the anatomical and physiological characterization of PrCnF neurons (Fig. 5A-C). We found that the dendrite number does not correlate with the dorsoventral location of the soma: ventrally located neurons had less dendrites ( $r^2 = 0.488$ ;  $p = 0.008$ ;  $n = 7$ ; Fig. 5D). Intriguingly, the amplitude of the persistent Na<sup>+</sup> current had no correlation with the input resistance ( $r^2 = 0.25$ ;  $p = 0.0683$ ) but with the soma area (the greater soma area had greater persistent Na<sup>+</sup> current;  $r^2 = 0.807$ ;  $p = 0.0383$ ;  $n = 5$ ; Fig. 5C, E). There is correlation between the dendrite number and the input resistance: cells with less dendrites had greater input resistance ( $r^2 = 0.579$ ;  $p = 0.0468$ ). In contrast to the expectations based on the physical principles, the amplitude of the A-current directly and not inversely correlated with the input resistance ( $r^2 = 0.346$ ;  $p = 0.0102$ ;  $n = 18$ ; Fig. 5A, F), indicating that a gradient is present from cells possessing A-current with greater amplitude and higher input resistance to cells with lower A-current amplitude and input resistance. Intriguingly, this relationship was not observed in the other nuclei ( $r^2 = 0.0042$ ,  $p = 0.768$  for the PPN and  $r^2 = 0.00249$ ,  $p = 0.808$  for the CnF). The decay tau of the A-current determines the delay of the first action potential (see above) and it is directly proportional to the slow afterhyperpolarization ( $r^2 = 0.456$ ,  $p = 0.0081$ ;  $n = 12$ ) in the PrCnF but not in the PPN ( $r^2 = 0.007$ ,  $p = 0.764$ ;  $n = 12$ ) and in the CnF ( $r^2 = 0.019$ ,  $p = 0.746$ ;  $n = 8$ ). No correlation was found between the persistent Na<sup>+</sup> current and the A-current amplitude ( $r^2 = 0.0314$ ,  $p = 0.562$ ) or decay tau ( $r^2 = 0.18$ ,  $p = 0.194$ ) in the PrCnF.

Certain expected correlations were also found: the medium and slow afterhyperpolarizations were directly proportional in the PrCnF ( $r^2 = 0.448$ ,  $p = 0.0063$ ;  $n = 15$ ; Fig. 5B, G). In the other nuclei, this relationship was also present in the PPN ( $r^2 = 0.197$ ,  $p = 0.0139$ ) but not in the CnF ( $r^2 = 0.269$ ,  $p = 0.124$ ). The input resistance (as expected from Ohm's law) determined voltage changes of the cell: the amplitudes of fast, medium and slow afterhyperpolarizations directly correlated with the input resistance (fAHP:  $r^2 = 0.364$ ,  $p = 0.0172$ ; mAHP:  $r^2 = 0.705$ ,  $p = 0.0001$ ; sAHP:  $r^2 = 0.342$ ,  $p = 0.028$ ;  $n = 15-15$  for fast and medium,  $n = 13$  for slow afterhyperpolarization; Fig. 5B, H). This relationship was neither seen in the CnF (fAHP:  $r^2 = 0.314$ ,  $p = 0.073$ ; mAHP:  $r^2 = 0.227$ ,  $p = 0.139$ ; sAHP:  $r^2 = 0.0082$ ,  $p = 0.803$ ;  $n = 11$ , 11 and 9, respectively), nor in the PPN (fAHP:  $r^2 = 0.021$ ,  $p = 0.156$ ; mAHP:  $r^2 = 0.0085$ ,  $p = 0.6271$ ; sAHP:  $r^2 = 0.056$ ,  $p = 0.216$ ;  $n = 27$ , 31 and 29, respectively). The first interspike interval was strongly and inversely correlated with the firing frequency in all nuclei (PrCnF:  $r^2 = 0.796$ ,  $p < 0.001$ ;  $n = 16$ ; Fig. 5C, I; CnF:  $r^2 = 0.427$ ,  $p = 0.0033$ ;  $n = 18$ ; PPN:  $r^2 = 0.154$ ,  $p = 0.0069$ ;  $n = 42$ ).

In conclusion, -out of the expected correlations based on the definitions of basic electrophysiological parameters- functional subgroups of PrCnF glutamatergic neurons could potentially be differentiated on the basis of the presence or absence of the A-current and the persistent Na<sup>+</sup> current among, but further evidence is necessary to support this claim.

### Age-dependence of the recorded parameters

To be able to compare our data with published studies on CnF and PPN glutamatergic neurons, we performed recordings on juvenile mice. Because the young age of the mice could potentially reveal age-related differences among MLR neurons, we obtained recordings from 7th and 17th postnatal days. No differences were observed in most parameters tested, with the exception of the frequency of high threshold membrane potential oscillations

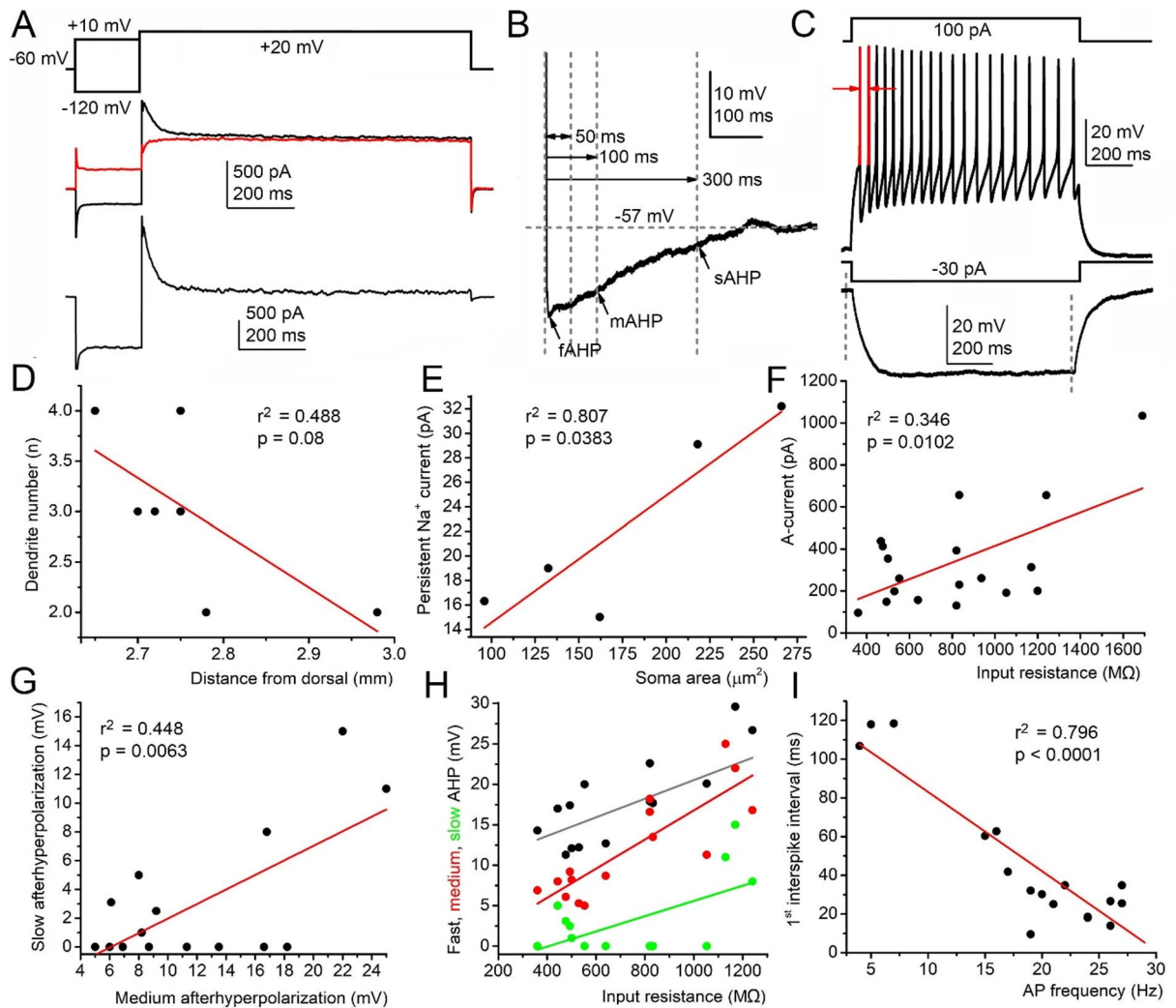


**Fig. 5.** Correlation of morphological and functional parameters in PrCnF neurons. **(A)** Representative traces of the A-current. Voltage protocols for recording of the current (above), current traces recorded with  $-120$  (black) and  $+10$  mV prepulse (middle) and the difference between the black and red curves (below). **(B)** Representative voltage trace demonstrating the measurement of the fast, medium and slow afterhyperpolarizations (fAHP, mAHP and sAHP, respectively). The resting membrane potential and the points for measurements are indicated with gray dashed lines. **(C)** Protocols and representative voltage traces for determining the first interspike interval (upper trace, red arrows and action potentials) and the input resistance (below). The points for measurements are indicated with gray dashed lines. **(D)** Correlation between the dorsoventral location of the soma and the number of dendrites. **(E)** Correlation of persistent  $\text{Na}^+$  current amplitude and soma area. Dots: individual data; lines: linear fits of the datasets. **(F)** Relationship between the input resistance and the A-current amplitude. **(G)** Correlation of the medium and slow afterhyperpolarizations. **(H)** Correlations of the input resistance and the fast, medium and slow afterhyperpolarizations (black, red and blue, respectively). fAHP:  $r^2 = 0.364, p = 0.0172$ ; mAHP:  $r^2 = 0.705, p = 0.0001$ ; sAHP:  $r^2 = 0.342, p = 0.028$ . **(I)** Correlation of the frequency and first interspike interval.

evoked with a depolarizing ramp protocol, which had a tendency to increase with age ( $r^2 = 0.311, p = 0.038, n = 13$  for the PrCnF;  $n = 32$  for the CnF and PPN; Fig. 6A–B), and the amplitude of the afterhyperpolarization, which increased with age. The linear fit of the dataset of the AHP from PrCnF neurons also revealed correlations of the fast and medium, but not in the slow AHP (fAHP:  $r^2 = 0.391, p = 0.004$ ; mAHP:  $r^2 = 0.286, p = 0.0183$ ; sAHP:  $r^2 = 0.209, p = 0.0559$ ; Fig. 6C–D). In contrast, the linear fit of the pooled dataset from the CnF and PPN showed no correlation (fAHP:  $r^2 = 0.07941, p = 0.0743$ ; mAHP:  $r^2 = 0.0716, p = 0.0867$ ; sAHP:  $r^2 = 0.0225, p = 0.356$ ; Fig. 6B, D).

## Discussion

In this study, we aimed to identify the morphological and functional properties of precuneiform nucleus (PrCnF) glutamatergic neurons, an understudied structure within the mesencephalic locomotor region (MLR). We compared the properties of PrCnF neurons with neighboring cuneiform nucleus (CnF) and pedunculopontine

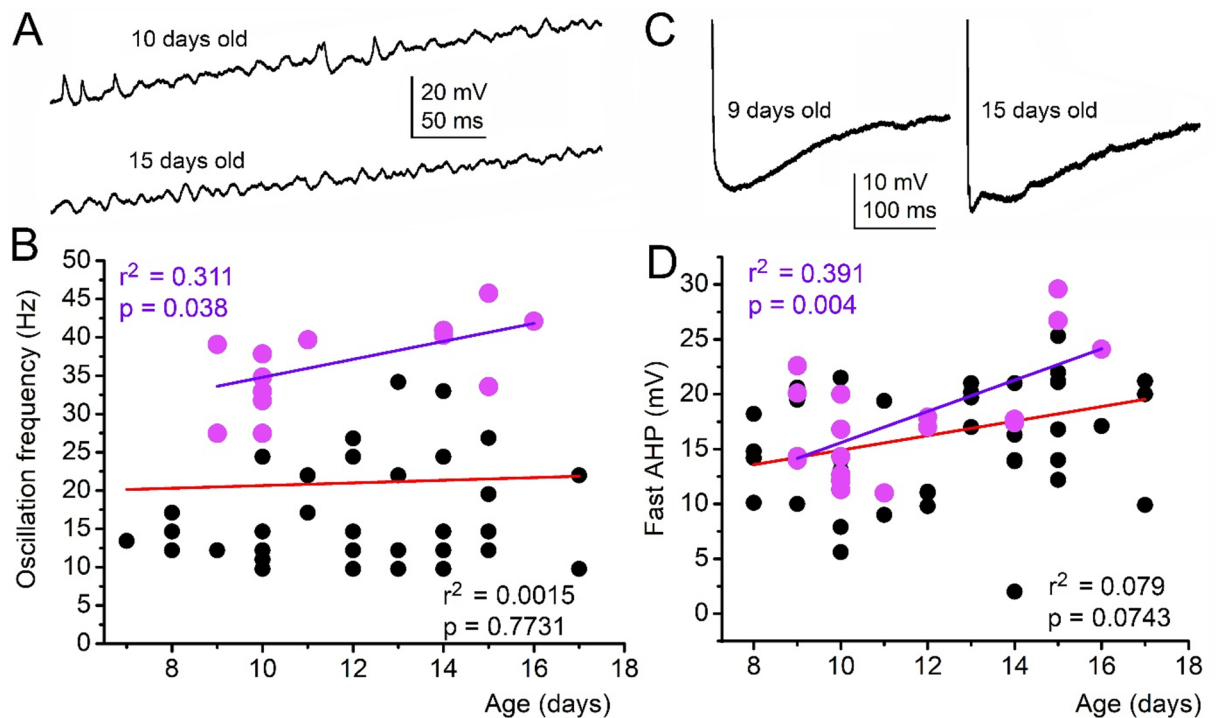


**Fig. 6.** Age-dependence of a subset of electrophysiological parameters in the PrCnF. **(A)** Representative voltage traces of high threshold membrane potential oscillations elicited by ramp depolarization on 10- and 15-days old mice. **(B)** Age-dependence of the oscillation frequency in the PrCnF (purple dots: individual data, dark purple line: linear fit) and in the PPN and CnF (black dots: individual data, red line: linear fit of all datapoints). **(C)** Afterhyperpolarizations of a 9- and a 15-days old mouse in the PrCnF. **(D)** Statistical demonstration of the age dependence of the fast afterhyperpolarization with a similar arrangement as on panel B (purple dots: datapoints from the PrCnF, dark purple line: linear fit of the datapoints from the PrCnF, black dots: datapoints from the PPN and the CnF, red line: linear fit of the datapoints indicated with black).

nucleus (PPN) glutamatergic neurons and found several distinctions among MLR neurons: (1) the dendritic morphology of PrCnF neurons is similar to PPN neurons but distinct from CnF neurons; (2) PrCnF neurons exhibit higher firing rates and oscillatory activity compared to CnF and PPN neurons; (3) unlike PPN and CnF neurons, the majority of PrCnF neurons did not show depolarization-related changes in spike frequency adaptation; and (4) the presence or absence of the A-current and the persistent  $\text{Na}^+$  current define functional subgroups within the PrCnF. Our findings support the notion of functional heterogeneity among MLR neurons and provide a fundamental description of the anatomical and electrophysiological properties of PrCnF neurons.

We first examined the morphological properties of PrCnF glutamatergic neurons. The dendritic morphology of PrCnF neurons resembled that of PPN neurons but differed from CnF neurons. Specifically, PrCnF neurons exhibited dendritic patterns similar to PPN neurons, suggesting possible similarities in their synaptic integration and connectivity. Dorsally located PrCnF neurons tended to have more dendrites, suggesting potential topographical variations within the nucleus, and display clear anatomical differences from CnF neurons. The somatodendritic parameters showed correlations with certain functional characteristics. The soma area was directly proportional to the amplitude of the persistent  $\text{Na}^+$  current, suggesting that larger neurons have greater persistent  $\text{Na}^+$  currents. Input resistance inversely correlates with cell size<sup>19</sup> and was correlated with A-current amplitude (see below). These findings indicate a relationship between somatic and functional parameters in PrCnF neurons.

Differences and overlaps in somatodendritic morphology might indicate similar relationships of the connectivity. An important limitation of our study is that only the somatodendritic morphology of the neurons was studied. In the future work, the axonal arborization and projections, as well as the connectivity of the nucleus are worth studying, which might not reveal fundamental differences but different weight and proportions of connections.

The outputs from the PrCnF target the ipsilateral cervical and upper thoracic spinal cord<sup>1,15</sup> and receives innervation from the central amygdala<sup>8</sup>. The connectivity of the CnF and PPN are well described in several studies. In brief, these nuclei have several overlaps in inputs and outputs, but PPN neurons possess more widespread connections than CnF with the spinal cord, the brainstem, cortical and subcortical areas. The areas where the CnF have more projections than PPN are the hypothalamus and the habenula<sup>5,20</sup>. The connectivity of the PrCnF with the amygdala and spinal cord, therefore, overlaps with the connectivity of the other MLR nuclei<sup>5,21</sup>.

Next, we investigated the electrophysiological properties of PrCnF neurons and compared them with CnF and PPN glutamatergic neurons. Functional subtypes within PPN cholinergic and glutamatergic neurons, as well as CnF glutamatergic neurons, have been classified based on *in vitro* properties<sup>10,22</sup>. In terms of classical functional groups—Type I, II, III, and IIIK neurons<sup>5,14</sup>—all nuclei exhibited similar heterogeneity, with slight differences due to varying proportions of neurons with and without A-current. Ionic currents determining firing patterns include the A-current, M-current, and persistent Na<sup>+</sup> current. The A-current, a transient K<sup>+</sup> current, prolongs the delay of the first action potential or the first interspike interval<sup>23</sup>. In PrCnF glutamatergic neurons, we observed a strong correlation between the A-current decay tau and the first action potential delay, indicating that the A-current drives the first AP delay, similar to PPN cholinergic neurons. Since the A-current is sensitive to inflammatory conditions<sup>24</sup>, the firing pattern of PrCnF glutamatergic and PPN cholinergic neurons may be affected by neuroinflammation. The M-current, a slowly activating K<sup>+</sup> current without inactivation, contributes to spike frequency adaptation and affects resting membrane potential and excitability<sup>25,26</sup>. Previously, we showed that PPN cholinergic neurons possess M-current, whereas GABAergic neurons lack it<sup>18</sup>. In CnF and PrCnF, 20–30% of glutamatergic neurons have M-current, indicating that cholinergic neuromodulation on excitability and firing pattern is weakest in PPN glutamatergic neurons and potentially stronger in CnF and PrCnF.

We then classified neurons into non-adapting, slowly adapting, and fast adapting types based on changes in spike frequency adaptation (SFA) with increasing depolarization<sup>5</sup>. Our findings revealed fundamental differences between CnF and PrCnF neurons: while CnF neurons were mostly fast adapting, the majority of PrCnF neurons were non-adapting, indicating potentially different roles in locomotion regulation. PrCnF neurons were distinguished by their higher firing rates and oscillatory activity compared to CnF and PPN neurons; their firing rate was significantly higher than that of CnF neurons and correlated with TTX-sensitive high-threshold membrane potential oscillations mediated by the persistent Na<sup>+</sup> current, which we demonstrated to be present in the majority of PrCnF neurons. In contrast, PPN neurons exhibited several subgroups in terms of adaptation, and while fast adapting neurons dominated in CnF, non-adapting neurons were predominant in PrCnF. Different nuclei and neuronal populations within the MLR exert various roles on movement and muscle tone: electrical stimulation of the CnF elicits locomotion, whereas stimulation of the PPN can increase or decrease muscle tone and exploratory locomotion<sup>3,5</sup>. Selective activation of CnF glutamatergic neurons induces locomotion with a speed proportional to stimulation frequency, while activation of MLR GABAergic neurons inhibits locomotion, and cholinergic stimulation produces ambiguous results in locomotor activity<sup>4,5,27,28</sup>. Comparing glutamatergic neuronal populations of the CnF and PPN reveals important differences: CnF neurons stimulate locomotion with firing rates that correlate linearly with locomotion speed, whereas PPN glutamatergic neurons are related to exploratory movements or cessation of ongoing movement while maintaining readiness for initiating new voluntary movement<sup>4,5</sup>. In PPN, the correlation between firing rate and locomotion speed is more complex, with some neurons showing a linear correlation, others showing no correlation, and a third population firing at the beginning of movement with decreased firing rate as speed increases. These results suggest that PrCnF neurons may have a uniform relationship to movement speed similar to CnF neurons, and that activation of the PrCnF might be related to higher-speed movements due to their weak spike frequency adaptation even during strong depolarization and higher firing rates compared to CnF and PPN neurons. Future *in vivo* studies will help to validate these speculations.

Subgroups within MLR neurons were recently identified by projection and expression of different factors. The Rbp4-positive neurons project to the basal ganglia and are active during forelimb movements<sup>29</sup>, whereas PPN Chx10<sup>+</sup> neurons produce motor arrest of ongoing movements and elicit autonomic changes<sup>30,31</sup>.

Furthermore, projections of the basal ganglia to various PPN populations differ in short term synaptic plasticity. Synapses with distinct properties of plasticity differentially affect behavioral properties as place preference and distance traveled<sup>32</sup>.

Correlating these or other neuronal populations determined by *in vivo* function, projection and markers with the membrane properties above is a possible future direction of the research on the PrCnF.

In this study, correlations with *in vivo* parameters, synaptic currents and *ex vivo* membrane properties were out of scope of our project and therefore not matched. Performing these experiments might increase understanding of the significance of the functional subpopulations of the PrCnF glutamatergic neurons described by us.

Another possible limitation of this study is the involvement of juvenile mice in the experiment. As several studies including our previous publication on the PPN and CnF uses animals with this age, a similar range of age was used for the possibility of comparison. No age-dependence was observed except for frequency of high threshold membrane potentials and the afterhyperpolarization. Therefore, at this point it is not possible to ascertain whether differences in membrane potential oscillations among MLR nuclei will preserve through adulthood.

In conclusion, glutamatergic populations of MLR nuclei show a number of overlapping morphological and functional properties, but PrCnF neurons can be distinguished by their unique firing properties and morphological characteristics. Understanding these *ex vivo* properties aids in designing *in vivo* experiments and exploring the potential of using this nucleus as a target for deep brain stimulation (DBS). The PPN is already a target of DBS in Parkinson's disease (PD), where DBS can alleviate pathological symptoms by reducing neuronal oscillations that promote destabilization<sup>33</sup>. Further research on the function of PrCnF glutamatergic neurons may therefore contribute to the design of *in vivo* studies and testing whether this area can serve as an alternative DBS target.

## Materials and methods

Patch clamp experiments were performed in normal artificial cerebrospinal fluid (naCSF) with the composition below (in mM): NaCl, 120; NaHCO<sub>3</sub>, 26; glucose, 10; myo-inositol, 3; KCl, 2.5; NaH<sub>2</sub>PO<sub>4</sub>, 1.25; sodium-pyruvate, 2; ascorbic acid, 0.5; CaCl<sub>2</sub>, 2; MgCl<sub>2</sub>, 1; pH 7.4. For preparation of brain slices, the Na<sup>+</sup> concentration

was reduced by replacement of 95 mM NaCl with 60 mM glycerol. This solution is referred as low Na<sup>+</sup> aCSF. Chemicals were purchased from Sigma-Aldrich (St. Louis, MO, USA), unless stated otherwise.

Experiments on mice were in accordance with the appropriate international (EU Directive 2010/63/EU for animal experiments), national and institutional guidelines and law on the care of research animals. The experimental protocols were approved by the Hungarian National Food Chain Safety Office (HB/06-ÉLB/129-1/2020).

7–18 days old mice with different genotypes were used. The average age was  $11.36 \pm 0.47$  days. (For previous recordings on the CnF, the average age was  $10.95 \pm 0.45$  days, for the PPN  $10.98 \pm 0.54$  days). Animals from both sexes expressing tdTomato fluorescent protein in a type 2 vesicular glutamate transporter- (Vglut2) dependent way were used for slice preparations ( $n = 16$ ). The homozygous Vglut2-cre (*Slc17a6<sup>tm2(cre)Lowl</sup>* (also called Vglut2-ires-Cre); Jax number: 028863) and floxed-stop- tdTomato (B6;129S6-Gt(ROSA)26Sor<sup>tm9(CAG-tdTomato)Hze/J</sup>; Jax mice accession number: 007905) strains were purchased from Jackson Laboratories (Bar Harbor, ME, USA) and crossed in the animal facility of the department. Mice were sacrificed with cervical dislocation. Coronal midbrain slices (with 200  $\mu$ m thickness) were prepared in ice-cold (0 - -2 °C) low Na<sup>+</sup> aCSF with a Microm HM 650 V vibratome (Microm International GmbH, Walldorf, Germany). Prior to starting slice electrophysiology experiments, slices were incubated in normal aCSF for 1 h on 37 °C.

All experiments were conducted on neurons expressing tdTomato fluorescent marker. Visualization of tdTomato was achieved with Till Photonics fluorescent imaging system (Till Photonics GmbH, Gräfeling, Germany) containing a xenon bulb-based Polychrome V light source, a CCD camera (SensiCam, PCO AG, Kelheim, Germany), an imaging control unit (ICU), and the Till Vision software (version 4.0.1.3).

To eliminate action potentials, 1  $\mu$ M tetrodotoxin (TTX; Alomone Laboratories, Jerusalem, Israel) was used in certain experiments.

Patch pipettes with 6–8 M $\Omega$  were fabricated with Narishige PP-830 pipette puller from borosilicate glass capillaries. The composition of the pipette solution was the following (in mM): K-gluconate, 120; NaCl, 5; 4-(2-hydroxyethyl)-1-piperazineethanesulfonic acid (HEPES), 10; Na<sub>2</sub>-phosphocreatinine, 10; EGTA, 2; CaCl<sub>2</sub>, 0.1; Mg-ATP, 5; Na<sub>3</sub>-GTP, 0.3; biocytin, 8; pH 7.3. Whole-cell patch-clamp experiments were conducted with an Axopatch 200 A amplifier (Molecular Devices, Union City, CA, USA) at room temperature. Data acquisition was achieved by Clampex 10.0 software (Molecular Devices, Union City, CA, USA), while Clampfit 10.0 (Molecular Devices) software was employed for data analysis. Only stable recordings with minimal leak currents were considered, and only recordings with series resistance below 25 M $\Omega$ , with less than 10% change were included.

Voltage- and current-clamp protocols and parameters recorded are represented in Table 1.

Neurons were labelled with biocytin administered in the pipette solution. Slices were fixed with 4% paraformaldehyde in 0.1 M phosphate buffer (pH 7.4; 4 °C). For permeabilization, Tris buffered saline (in mM, Tris base, 8; Trisma HCl, 42; NaCl, 150; pH 7.4) with additional 0.1% Triton X-100 and 10% bovine serum (60 min) was used. Streptavidin-conjugated Alexa488 (1:300; Molecular Probes Inc., Eugene, OR, USA) dissolved in phosphate buffer was administered for 90 min. Fluorescent signals were visualized using a Zeiss LSM 510 confocal microscope (Carl Zeiss AG); images were taken with 20x objective and 1  $\mu$ m z stacks. The NeuroLucida software (MBF Bioscience, Williston, VT, USA) was used for reconstruction of neurons and assessment of somatodendritic parameters and locations.

Functional and morphological data from the PPN and the CnF have been previously published by us<sup>5</sup>. Data were re-analyzed and used for comparison with the PrCnF in order to assess the potential differences or similarities in the parameters of the neighboring nuclei.

All data represent mean  $\pm$  SEM. Statistical analysis was performed with Excel (Microsoft, Redmont, WA, USA) and Prism software (GraphPad Software, Boston, MA, USA). After initial assessment of the normal distribution of the datasets by normality tests, Student's t-test was applied for comparison of two datasets. Multiple comparisons were analyzed with Dunn's test. The linear correlation between independent datasets was assessed by using the Pearson's correlation coefficient ( $r$ ). In all cases, the level of significance was  $p < 0.05$ .

	Protocol	Recorded parameter
<b>Voltage clamp protocols</b>		
Persistent sodium current	2.5 s long depolarizing voltage ramp from -80 mV holding potential to -5 mV	Amplitude of TTX-sensitive inward current activated between -40 and -20 mV
A-current	1 s long depolarizing voltage steps to +20 mV, preceded with a 200 ms long hyperpolarizing voltage step to -120 mV or a depolarizing voltage step to +10 mV from the holding potential of -60 mV	Amplitude of the transient outward current recorded from the difference of the two traces with different prepulses
M-current	1 s long repolarizing voltage steps from -20 mV holding potential from -60 mV with 10 s increment	Difference of the instantaneous and steady state currents on each sweeps
<b>Current clamp protocols</b>		
Input resistance	1 s long current steps from -30 to +120 pA with 10 s increment. The membrane potential was set to different values between -50 and -90 mV with 10 mV increment.	Calculated from the steady state voltage response to -30 pA current injection
Depolarization sag		Calculated as the difference of the maximal hyperpolarization and the steady state voltage response to -30 pA current injection
Action potential firing frequency		Number of action potentials during the 1 s long current injection
Frequency of the action potential train		Fraction of action potential number and the duration of the action potential train
Duration of the action potential train		Time between the first and last action potentials
Ratio of the last and first action potential amplitudes		Fraction of the first and last action potential amplitudes measured as the voltage differences between the firing thresholds and peak potentials
Ratio of the last and first action potential durations		Fraction of the first and last action potential durations measured as the time differences between the firing threshold and a point of the declining phase reaching the voltage value of the threshold
Delay of the first action potential		Time difference between the beginning of the current step and the peak potential of the first action potential at the sweep recorded with 100 pA depolarizing current injection
Fast, medium and slow afterhyperpolarization (fAHP, mAHP, sAHP, respectively)		Action potentials elicited by rheobase depolarizing current (+20 -+60 pA) were assessed. fAHP was defined as the greatest hyperpolarization peak within 50 ms from the peak potential of the action potential. mAHP was measured at 100 ms, sAHP was recorded after 300 ms after the peak potential.
Adaptation index		$AI = 1 - (F_{last} / F_{initial})$ $F_{last}$ = average frequency of the last 2 action potentials $F_{initial}$ = average frequency of the first 3 action potentials [26]
Calcium hump		Maximal voltage difference of the transient depolarization and the average steady state voltage at the last 100 ms of the depolarizing step; measured in the presence of TTX
Calcium rebound		Maximal voltage difference of the transient depolarization following the hyperpolarizing voltage steps and the resting membrane potential measured as the average voltage of a 100 ms long trace preceding the voltage step
TTX-sensitive high threshold membrane potential oscillations		Power spectrum of the voltage changes elicited by +120 pA current injection, before and during TTX application
TTX-resistant high threshold membrane potential oscillations	Power spectrum of the voltage changes elicited by ramp current injection in the presence of TTX	

**Table 1.** Voltage- and current clamp protocols and recorded parameters.

## Data availability

All data are available in the manuscript text.

Received: 8 January 2025; Accepted: 17 October 2025

Published online: 21 November 2025

## References

- Liang, H., Paxinos, G. & Watson, C. Spinal projections from the presumptive midbrain locomotor region in the mouse. *Brain Struct. Funct.* **217** (2), 211–219. <https://doi.org/10.1007/s00429-011-0337-6> (2012).
- Coles, S. K., Iles, J. F. & Nicolopoulos-Stournaras, S. The mesencephalic centre controlling locomotion in the rat. *Neuroscience*. **28**(1), 149–57 [https://doi.org/10.1016/0306-4522\(89\)90239-x](https://doi.org/10.1016/0306-4522(89)90239-x) (1989).
- Takakusaki, K., Chiba, R., Nozu, T. & Okumura, T. Brainstem control of locomotion and muscle tone with special reference to the role of the mesopontine tegmentum and medullary reticulospinal systems. *J. Neural Transm. (Vienna)*. **123** (7), 695–729. <https://doi.org/10.1007/s00702-015-1475-4> (2016).
- Caggiano, V. et al. Midbrain circuits that set locomotor speed and gait selection. *Nature* **553** (7689), 455–460. <https://doi.org/10.1038/nature25448> (2018).
- Dautan, D. et al. Modulation of motor behavior by the mesencephalic locomotor region. *Cell. Rep.* **24** (8), 109594. <https://doi.org/10.1016/j.celrep.2021.109594> (2021).
- Noga, B. R. & Whelan, P. J. The mesencephalic locomotor region: beyond locomotor control. *Front. Neural Circuits*. **16**, 884785. <https://doi.org/10.3389/fncir.2022.884785> (2022).
- Korte, S. M., Jaarsma, D., Luiten, P. G. & Bohus, B. Mesencephalic cuneiform nucleus and its ascending and descending projections serve stress-related cardiovascular responses in the rat. *J. Auton. Nerv. Syst.* **41** (1–2). [https://doi.org/10.1016/0165-1838\(92\)90137-6](https://doi.org/10.1016/0165-1838(92)90137-6) (1992). 157–76.

8. Liang, H., Watson, C. & Paxinos, G. Projections from the oral Pontine reticular nucleus to the spinal cord of the mouse. *Neurosci. Lett.* **584**, 113–118. <https://doi.org/10.1016/j.neulet.2014.10.025> (2015).
9. Roussel, M., Lafrance-Zoubga, D., Josset, N., Lemieux, M. & Bretzner, F. Functional contribution of mesencephalic locomotor region nuclei to locomotor recovery after spinal cord injury. *Cell. Rep. Med.* **4** (2), 100946. <https://doi.org/10.1016/j.xcrim.2023.100946> (2023).
10. Kang, Y. & Kitai, S. T. Electrophysiological properties of pedunculopontine neurons and their postsynaptic responses following stimulation of substantia nigra reticulata. *Brain Res.* **3** (1), 79–95. [https://doi.org/10.1016/0006-8993\(90\)91826-3](https://doi.org/10.1016/0006-8993(90)91826-3) (1990).
11. Mena-Segovia, J., Sims, H. M., Magill, P. J. & Bolam, J. P. Cholinergic brainstem neurons modulate cortical gamma activity during slow oscillations. *J. Physiol.* **15** (12), 2947–2960. <https://doi.org/10.1113/jphysiol.2008.153874> (2008).
12. Ros, H., Magill, P. J., Moss, J., Bolam, J. P. & Mena-Segovia, J. Distinct types of non-cholinergic pedunculopontine neurons are differentially modulated during global brain states. *Neuroscience* **29**;170 (1), 78–91. <https://doi.org/10.1016/j.neuroscience.2010.06.068> (2010).
13. Kroeger, D. et al. Cholinergic, glutamatergic, and GABAergic neurons of the pedunculopontine tegmental nucleus have distinct effects on sleep/wake behavior in mice. *J. Neurosci.* **37** (5), 1352–1366. <https://doi.org/10.1523/JNEUROSCI.1405-16.2016> (2017).
14. Baksa, B. et al. Characterization of functional subgroups among genetically identified cholinergic neurons in the pedunculopontine nucleus. *Cell. Mol. Life Sci.* **76** (14), 2799–2815. <https://doi.org/10.1007/s00018-019-03025-4> (2019).
15. Liang, H., Paxinos, G. & Watson, C. Projections from the brain to the spinal cord in the mouse. *Brain Struct. Funct.* **215** (3–4), 159–186. <https://doi.org/10.1007/s00429-010-0281-x> (2011).
16. Paxinos, G. & Franklin, K. B. *The Mouse Brain in Stereotaxic Coordinates* 4th edn (Elsevier, 2013).
17. Ryczko, D. The mesencephalic locomotor region: multiple cell types, multiple behavioral roles, and multiple implications for disease. *Neuroscientist* **30** (3), 347–366. <https://doi.org/10.1177/10738584221139136> (2024).
18. Bordas, C., Kovacs, A. & Pal, B. The M-current contributes to high threshold membrane potential oscillations in a cell type-specific way in the pedunculopontine nucleus of mice. *Front. Cell. Neurosci.* **9**, 121. <https://doi.org/10.3389/fncel.2015.00121> (2015).
19. Cuntz, H. et al. A general principle of dendritic constancy: A neuron's size- and shape-invariant excitability. *Neuron* **109** (22), 3647–3662e7. <https://doi.org/10.1016/j.neuron.2021.08.028> (2021).
20. Mena-Segovia, J. & Bolam, J. P. Rethinking the pedunculopontine nucleus: from cellular organization to function. *Neuron* **94** (1), 7–18. <https://doi.org/10.1016/j.neuron.2017.02.027> (2017).
21. Özkan, M. et al. Non-motor connections of the pedunculopontine nucleus of the rat and human brain. *Neurosci. Lett.* **767**, 136308. <https://doi.org/10.1016/j.neulet.2021.136308> (2022).
22. Leonard, C. S. & Llinás, R. Serotonergic and cholinergic inhibition of mesopontine cholinergic neurons controlling REM sleep: an in vitro electrophysiological study. *Neuroscience* **59** (2), 309–330. [https://doi.org/10.1016/0306-4522\(94\)90599-1](https://doi.org/10.1016/0306-4522(94)90599-1) (1994).
23. Kanold, P. O. & Manis, P. B. Transient potassium currents regulate the discharge patterns of the dorsal cochlear nucleus pyramidal cells. *J. Neurosci.* **19** (6), 2195–2208. <https://doi.org/10.1523/JNEUROSCI.19-06-02195.1999> (1999).
24. Monnerat-Cahli, G. et al. Toll-like receptor 4 activation promotes cardiac arrhythmias by decreasing the transient outward potassium current (I<sub>to</sub>) through an IRF3-dependent and MyD88-independent pathway. *J. Mol. Cell. Cardiol.* **76**, 116–125. <https://doi.org/10.1016/j.yjmcc.2014.08.012> (2014).
25. Brown, D. A., Passmore, G. M. & Neural, K. C. N. Q. Kv7 channels. *Br. J. Pharmacol.* **156** (8), 1185–1195. <https://doi.org/10.1111/j.1476-5381.2009.00111.x> (2009).
26. Nigro, M. J., Mateos-Aparicio, P. & Storm, J. F. Expression and functional roles of Kv7/KCNQ/M-channels in rat medial entorhinal cortex layer II stellate cells. *J. Neurosci.* **34** (20), 6807–6812. <https://doi.org/10.1523/JNEUROSCI.4153-13.2014> (2014).
27. Roseberry, T. K. et al. Cell-type-specific control of brainstem locomotor circuits by basal ganglia. *Cell* **164** (3), 526–537. <https://doi.org/10.1016/j.cell.2015.12.037> (2016).
28. Gut, N. K. & Mena-Segovia, J. Midbrain cholinergic neurons signal negative feedback to promote behavioral flexibility. *Trends Neurosci.* **45** (7), 502–503. <https://doi.org/10.1016/j.tins.2022.04.005> (2022).
29. Ferreira-Pinto, M. J. et al. Functional diversity for body actions in the mesencephalic locomotor region. *Cell* **184** (17), 4564–4578e18. <https://doi.org/10.1016/j.cell.2021.07.002> (2021).
30. Goñi-Erro, H., Selvan, R., Caggiano, V., Leiras, R. & Kiehn, O. Pedunculopontine Chx10<sup>+</sup> neurons control global motor arrest in mice. *Nat. Neurosci.* **26**(9), 1516–1528. <https://doi.org/10.1038/s41593-023-01396-3>. Erratum in: *Nat. Neurosci.* **26**(9), 1651. <https://doi.org/10.1038/s41593-023-01422-4> (2023).
31. Huang, Y. et al. Glutamatergic circuits in the pedunculopontine nucleus modulate multiple motor functions. *Neurosci. Bull.* **40** (11), 1713–1731. <https://doi.org/10.1007/s12264-024-01314-y> (2024).
32. Fallah, M., Udobi, K. C., Swiatek, A. E., Scott, C. B. & Evans, R. C. Inhibitory basal ganglia nuclei differentially innervate pedunculopontine nucleus subpopulations and evoke differential motor and Valence behaviors. *eLife* **13**, RP102308. <https://doi.org/10.7554/eLife.102308.2> (2024).
33. French, I. T. & Muthusamy, K. A. A review of the pedunculopontine nucleus in parkinson's disease. *Front. Aging Neurosci.* **10**, 99. <https://doi.org/10.3389/fnagi.2018.00099> (2018).

## Acknowledgements

This work was funded by the National Research Development and Innovation Office (NKFIH-K146873 to BP). TB was supported by the Stipendium Hungaricum PhD programme.

## Author contributions

KP, TB, AC and BP performed most murine electrophysiological and morphological experiments, PS supervised the morphological analysis of the recorded neurons. JMS wrote the manuscript. BP initiated the project, analyzed the data and wrote the manuscript.

## Declarations

## Competing interests

The authors declare no competing interests.

## Ethical approval

The authors have declared that the study is reported in accordance with ARRIVE guidelines.

## Additional information

Correspondence and requests for materials should be addressed to B.P.

**Reprints and permissions information** is available at [www.nature.com/reprints](http://www.nature.com/reprints).

**Publisher's note** Springer Nature remains neutral with regard to jurisdictional claims in published maps and institutional affiliations.

**Open Access** This article is licensed under a Creative Commons Attribution-NonCommercial-NoDerivatives 4.0 International License, which permits any non-commercial use, sharing, distribution and reproduction in any medium or format, as long as you give appropriate credit to the original author(s) and the source, provide a link to the Creative Commons licence, and indicate if you modified the licensed material. You do not have permission under this licence to share adapted material derived from this article or parts of it. The images or other third party material in this article are included in the article's Creative Commons licence, unless indicated otherwise in a credit line to the material. If material is not included in the article's Creative Commons licence and your intended use is not permitted by statutory regulation or exceeds the permitted use, you will need to obtain permission directly from the copyright holder. To view a copy of this licence, visit <http://creativecommons.org/licenses/by-nc-nd/4.0/>.

© The Author(s) 2025